Spatial variability of the snowmelt–albedo feedback in Antarctica

C. L. Jakobs[1], C. H. Reijmer[1], M. R. van den Broeke[1]
W. J. van de Berg[1], J. M. van Wessem[1]

[1]Institute for Marine and Atmospheric Research Utrecht, Utrecht University, The Netherlands

Key Points:

- We use a regional climate model to quantify the snowmelt–albedo feedback for the Antarctic ice sheet
- We find that this feedback is most active on East Antarctic ice shelves
- Precipitation frequency, timing and summer air temperature are key parameters for its importance

Corresponding author: Stan Jakobs, c.l.jakobs@uu.nl

Abstract

Surface melt is an important process for the stability of ice shelves, and therewith the Antarctic ice sheet. In Antarctica, absorption of solar radiation is mostly the largest energy source for surface melt, which is further enhanced by the snowmelt–albedo feedback (SMAF): refrozen snow has a lower albedo than new snow, which causes it to absorb more solar radiation, further increasing the energy available for surface melt. This feedback has previously been shown to increase surface melt by approximately a factor of 2.5 at Neumayer Station in East Antarctica. In this study, we use a regional climate model to quantify SMAF for the entire Antarctic ice sheet. We find that it is most effective on ice shelves in East Antarctica, and is less important in the Antarctic Peninsula and on the Ross and Filchner-Ronne ice shelves. We identify a relationship between SMAF and average summer air temperatures, and find that SMAF is most important around 265±2 K. On a sub-seasonal scale, we identify several parameters that contribute to SMAF: the length of dry periods, the time between significant snowfall events and snowmelt events, and prevailing temperatures. We then apply the same temperature-dependency of SMAF to the Greenland ice sheet and find that it is potentially active in a narrow band around the ice sheet, and finally discuss how the importance of SMAF could change in a warming climate.

Plain Language Summary

The Antarctic ice sheet is surrounded by ice shelves: floating extensions that prevent it from flowing into the oceans. The stability of these ice shelves is mainly affected by the melting of snow and ice, leading to a potential disintegration of the entire ice shelf. To properly simulate the climate, models should therefore be able to accurately reproduce snowmelt rates. Snowmelt in Antarctica is mainly driven by the absorption of solar radiation. This is subject to a positive feedback: when snow melts, it becomes darker, causing it to absorb more radiation. This leads to more energy that is available for snowmelt, which further darkens the surface. In this study, we use a climate model to quantify the importance of this feedback for the Antarctic ice sheet. We find that it is most important in regions with an average summer air temperature around 265 K. We furthermore find that during a long, dry period in summer, the feedback is more effective, and that the timing between snowfall and snowmelt partly determines how much the feedback will affect snowmelt. As a final step, we estimate how important this feedback is in Greenland, and how the observed patterns could change in a warming climate.

1 Introduction

The Antarctic ice sheet (AIS) contains approximately 26 million km^3 of ice, equivalent to a global mean sea level change of 58 m (Morlighem et al., 2020). In recent years, accelerated mass loss from the AIS has been observed; Shepherd et al. (2018) report a mass loss rate of 109±56 Gt yr^{-1} over the period 1992–2017. The highest mass loss is observed in West Antarctica, as a result of the thinning and disappearing of ice shelves, the floating extensions of the grounded ice sheet. Ice shelves are present along ∼74 % of the AIS (Bindschadler et al., 2011), buttressing the grounded ice sheet. They experience basal melt through ocean–ice heat exchange (Pritchard et al., 2012; Massom et al., 2018), as well as surface melt by energy exchange at the ice-shelf surface (Van den Broeke, 2005; Kingslake et al., 2017). The recent collapse of Larsen A and B ice shelves on the east side of the Antarctic Peninsula (AP) was preceded by extensive surface melt, inducing hydrofracturing (Van den Broeke, 2005; Glasser & Scambos, 2008). On the west side of the AP, break-up events on Wilkins ice shelf have been associated with increased basal melt rates, leading to changes in buoyant forces (Braun et al., 2009; Padman et al., 2012). Ice-shelf thinning and break-up have both been associated with the acceleration of its feeding glaciers (Scambos et al., 2004; Rott et al., 2011), causing the high

mass loss rates in coastal West Antarctica and the AP (Wouters et al., 2015; Turner et al., 2017). Ice-shelf stability is thus crucial for the future mass balance of the AIS. Because both basal and surface melt are expected to increase in a warming climate also for the more southerly ice shelves (Trusel et al., 2015), a proper representation of ice-shelf melt processes is essential in climate modeling.

In this paper we focus on surface melt processes. Weather stations, satellites and climate models have been used to estimate surface melt rates on Antarctic ice shelves (Bromwich et al., 2013; Trusel et al., 2015; Van Kampenhout et al., 2017; Van Wessem et al., 2018; Agosta et al., 2019; Souverijns et al., 2019). In-situ observations show that in the cold climate of Antarctica, insolation is usually the most important energy source for surface melt (Van den Broeke, Reijmer, et al., 2005; Jonsell et al., 2012; King et al., 2015; Jakobs et al., 2020). The absorption of solar radiation is in turn enhanced by the snowmelt–albedo feedback (SMAF) (Jakobs et al., 2019): when snow melts, meltwater percolates into the subsurface snow layers where it can refreeze. As refrozen snow consists of larger snow grains than new snow, it reduces the backward scattering of photons (Wiscombe & Warren, 1980), i.e. it has a lower albedo. As a result, the surface absorbs more incoming solar radiation, leading to more surface melt, representing a positive feedback. Therefore, it is crucial for climate models to use a snow albedo parameterization that includes this melt–albedo feedback (Cullather et al., 2014; Van Dalum et al., 2019; Alexander et al., 2019).

In a previous study, we used high-quality meteorological observations from Neumayer Station, located on Ekström ice shelf in East Antarctica, to quantify the effect of SMAF on surface melt rates (Jakobs et al., 2019). We used a surface energy balance (SEB) model that includes a grain-size-dependent albedo parameterization, and found that on average, SMAF enhanced surface melt (1992–2016) at Neumayer Station by a factor of 2.5, but with significant interannual variability. The current study aims to extend our previous work to the entire AIS, using the regional climate model RACMO2. This climate model is specifically developed to simulate polar climates and has been extensively evaluated (Van Wessem et al., 2018; Jakobs et al., 2020). Its albedo parameterization makes it well-suited to study SMAF at the continental scale.

In the next section, we introduce the climate model RACMO2 and describe the albedo parameterization used. In Section 3 we present a map of SMAF in Antarctica (Section 3.1), discussing its spatial variability as well as the interannual variability at different locations (Section 3.2). We identify regions in Antarctica that are most affected by SMAF (Section 4.1) and present local case studies on a daily timescale to identify conditions where SMAF is largest (Section 4.2). In Section 4.3, we comment on the potential importance of SMAF in Greenland, and how SMAF will affect surface melt in the future on both ice sheets, followed by conclusions in Section 5.

2 Methods

2.1 Model descriptions

The regional climate model RACMO2 is developed by the Royal Netherlands Meteorological Institute (KNMI). It is a hydrostatic model that combines the dynamical core of the High Resolution Limited Area Model (HIRLAM, Undén et al. (2002)) with the physics parameterizations of the Integrated Forecast System (IFS, version CY33r1) of the European Centre for Medium-Range Weather Forecast (ECMWF) (ECMWF, 2008).

For this study, we use the latest polar version (RACMO2.3p2, from now on referred to as RACMO2), which has been specifically developed for use over glaciated regions (Reijmer et al., 2005; Van Wessem et al., 2018). The atmosphere is represented by 40 vertical levels and the model is forced by the ERA-Interim reanalysis product at its lateral boundaries as well as in the upper atmosphere (Van de Berg & Medley, 2016). The atmospheric

component is coupled to a multilayer snow model (Ettema et al., 2010), which allows for meltwater percolation, refreezing and runoff. Furthermore, RACMO2 uses an albedo parameterization that depends on grain size (Gardner & Sharp, 2010; Kuipers Munneke et al., 2011) and a drifting-snow scheme that simulates horizontal transport of snow by near-surface winds (Lenaerts et al., 2012).

Van Wessem et al. (2018) compared the output of RACMO2 with in-situ measurements of surface temperature, radiation fluxes, turbulent fluxes and wind speed. They found that RACMO2 yields reliable estimates of surface temperatures and net short-wave radiation ($R^2 > 0.9$), and performs adequately in modeling turbulent fluxes, net long-wave radiation and wind speed ($R^2 > 0.5$). They furthermore found a good correlation ($R^2 = 0.81$) of surface melt rates with the results from the QuikSCAT satellite. Jakobs et al. (2020) showed that RACMO2 reproduces surface melt rates with reasonable accuracy: compared to in-situ melt estimates from (automatic) weather stations in the AP and Dronning Maud Land, RACMO2 slightly underestimates surface melt rates (bias=-7.3 mm w.e. yr^{-1}) but overall, the agreement is good ($R^2 > 0.8$).

RACMO2 solves the surface energy balance (SEB) equation, which describes the energy exchange between the surface, the sub-surface and the atmosphere and determines the amount of energy available for surface melt:

$$\mathrm{M} = \mathrm{R_{net}} + Q_\mathrm{S} + Q_\mathrm{L} + Q_\mathrm{G}, \tag{1}$$

where $\mathrm{R_{net}}$ is net radiation, the sum of net short-wave and net long-wave radiation, Q_S and Q_L are the turbulent fluxes of sensible and latent heat, respectively, and Q_G is the surface value of the subsurface heat flux. M is the energy available for surface melt, which is equal to 0 when the surface temperature is below the melting point of ice (273.15 K). In an iterative procedure, the surface temperature is determined so that the SEB is closed. If this temperature would exceed 273.15 K, it is forced to this value and excess energy is available for surface melt. The turbulent fluxes Q_S and Q_L are determined using Monin-Obukhov similarity theory, which relates the fluxes to the near-surface gradients of wind speed, potential temperature and humidity (see e.g. Van den Broeke, Van As, et al. (2005)). The subsurface heat flux $Q_\mathrm{G} = k\frac{\partial T}{\partial z}$, where k is the effective thermal conductivity of the snow/ice and $\frac{\partial T}{\partial z}$ the temperature gradient in the near-surface snowpack. The snow model solves the heat-conductivity equation to obtain the subsurface temperature profile and therewith Q_G (Ettema et al., 2010):

$$\rho c_\mathrm{p} \frac{\partial T}{\partial t} = -\frac{\partial}{\partial z}\left(k\frac{\partial T}{\partial z}\right) + q_\mathrm{refr}, \tag{2}$$

where q_refr is the energy released by the refreezing of meltwater per unit time per area. Penetration of short-wave radiation is not considered in this version of RACMO2.

This version of RACMO2 uses the albedo parameterization of Gardner and Sharp (2010), in which the albedo is described as a base value α_S with modifications due the solar zenith angle θ ($\mathrm{d}\alpha_u$), the cloud optical thickness τ ($\mathrm{d}\alpha_\tau$) and the concentration of black carbon in the snow ($\mathrm{d}\alpha_c$). The impact of snow impurities is assumed negligible for Antarctica and thus $\mathrm{d}\alpha_c$=0 (Warren & Clarke, 1990; Grenfell et al., 1994; Bisiaux et al., 2012; Marquetto et al., 2020)).

The base albedo α_S is given by (Gardner & Sharp, 2010):

$$\alpha_\mathrm{S} = 1.48 - 1.27048 r_\mathrm{e}^{0.07}, \tag{3}$$

where r_e is the snow grain size, in turn parameterized as

$$r_\mathrm{e}(t) = \left[r_\mathrm{e}(t-1) + \mathrm{d}r_\mathrm{e,dry} + \mathrm{d}r_\mathrm{e,wet}\right] f_\mathrm{o} + r_\mathrm{e,0} f_\mathrm{n} + r_\mathrm{e,r} f_\mathrm{r}, \tag{4}$$

where $\mathrm{d}r_\mathrm{e,dry}$ and $\mathrm{d}r_\mathrm{e,wet}$ describe grain growth due to dry and wet snow metamorphism, respectively. $r_\mathrm{e,0}$ and $r_\mathrm{e,r}$ denote the grain sizes of new and refrozen snow, set to constant values of $r_\mathrm{e,0} = 54$ mm (Kuipers Munneke et al., 2011) and $r_\mathrm{e,r} = 1000$ mm (Van Wessem

et al., 2018). f_o, f_n and f_r are the fractions of old, new and refrozen snow. The effect of the second layer is considered by changing the base albedo α_S to:

$$\alpha'_\mathrm{S} = \left(\alpha_\mathrm{S}^\mathrm{btm} - \alpha_\mathrm{S}^\mathrm{top}\right) + A\left(\alpha_\mathrm{S}^\mathrm{top} - \alpha_\mathrm{S}^\mathrm{btm}\right), \tag{5}$$

where top and btm indicate the top and bottom layers respectively, and A is a factor dependent on $\alpha_\mathrm{S}^\mathrm{top}$ and the top-layer thickness z. Equations for $\mathrm{d}\alpha_u$, $\mathrm{d}\alpha_\tau$, $\mathrm{d}r_\mathrm{e,dry}$, $\mathrm{d}r_\mathrm{e,wet}$ and A can be found in Gardner and Sharp (2010). This approach is different from Kuipers Munneke et al. (2011) and Jakobs et al. (2019), who used more than two layers to calculate the surface albedo.

2.2 Quantifying SMAF

To quantify the effect of SMAF, we performed two simulations with RACMO2 on a 27 km horizontal resolution for the period 1979–2018: a baseline run R_0 in which the full albedo parameterization is used as described above, and a sensitivity run R_1, in which the contribution of refrozen snow to snow grain size, and hence surface albedo, is disabled by setting $f_\mathrm{r} = 0$ in Eq. (4). The same approach was used by Jakobs et al. (2019) to quantify SMAF at Neumayer Station in East Antarctica. The term 'period-average' is used throughout this article, referring to the period 1979–2018.

There are several ways to quantify SMAF. The most robust definition is $\mathrm{SMAF_t}$, the ratio of the total ('t') cumulative amounts of surface melt in R_0 and R_1 over the entire period available (in this study 1979–2018). We use this measure to interpret the spatial variability of SMAF and e.g. its correlation with period-average temperature. SMAF can also be determined on a seasonal ('s') basis, i.e. the ratio of seasonal (in this study Jul–Jun) melt in R_0 and R_1, and is denoted by $\mathrm{SMAF_s}$. Time series of $\mathrm{SMAF_s}$ are used to study the interannual variability of SMAF and the connection to the SEB.

3 Results

3.1 Spatial distribution of SMAF

Since SMAF is defined as the ratio of surface melt in two different runs, we first present the relation between seasonal surface melt rates and $\mathrm{SMAF_s}$ in Fig. 1a, for seasons with at least 10 mm w.e. of surface melt, for each model grid cell. The figure shows that the highest $\mathrm{SMAF_s}$ values occur in low-melt regions, while in high-melt regions $\mathrm{SMAF_t}$ is close to 1. It furthermore shows that melt is not the only driver of $\mathrm{SMAF_s}$. In this section we study the spatial distribution of SMAF and surface melt; in Sect. 4 we then discuss possible other drivers of SMAF.

To identify the regions where SMAF is most important, we first need to know the spatial distribution of surface melt in Antarctica. This is presented in Fig. 2a, with the highest values occurring on both sides of the AP, locally exceeding 300 mm w.e. yr^{-1}. Extreme values (>500 mm w.e. yr^{-1}) occur on small islands north of the AP. The highest surface melt rates in East Antarctica are found on Shackleton ice shelf (indicated in Fig. 2c with an 'S'), due to its northerly location. The lowest values are found on the Ross and Filchner-Ronne ice shelves. The absolute increase in seasonal average melt because of SMAF ($R_0 - R_1$) is shown in Fig. 2b. A pattern similar to Fig. 2a emerges, with the highest values in the AP and on Shackleton ice shelf, but also in coastal Dronning Maud Land and the Amundsen Sea sector.

Figure 2c shows the resulting $\mathrm{SMAF_t}$, ranging from 1 to ∼2.8, for locations with at least 5 mm w.e. of period-average seasonal surface melt. The highest values are found in coastal Dronning Maud Land and the Amundsen Sea sector; these locations have relatively low seasonal surface melt rates, combined with an increase because of SMAF that is relatively large. Lower values are found in low-melt regions such as on the Ross and

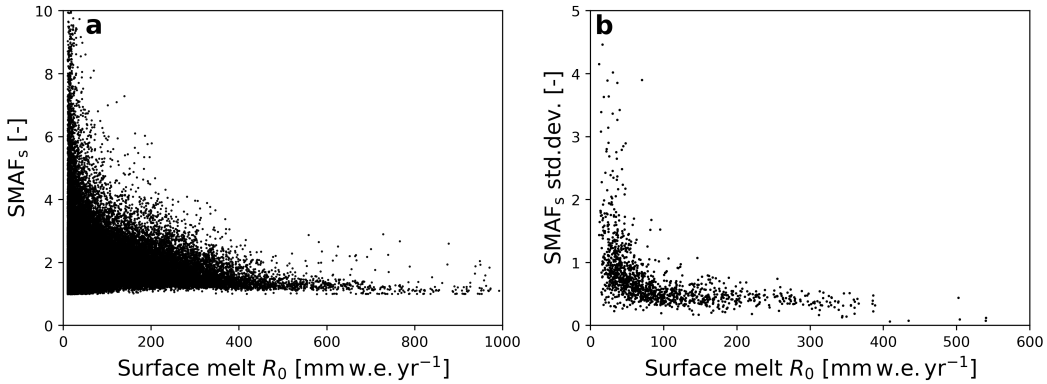

Figure 1. **a** Relationship between surface melt rate and SMAF$_s$. Each dot represents one season with at least 10 mm w.e. for all grid points within the model domain. **b** Period-average seasonal surface melt versus SMAF$_s$ standard deviation for all grid points with period-average seasonal surface melt ≥ 5 mm w.e.

Filchner-Ronne ice shelves, and high-melt regions such as the northern AP. These patterns are discussed in more detail in Sect. 4.1, but first we consider the temporal variability of SMAF$_s$.

3.2 Temporal variability of SMAF

For six locations, indicated by blue dots in Fig. 2c, time series of seasonal snow melt for both runs (R_0 and R_1) are presented in Fig. 3. The ratio between these two yields the seasonal SMAF$_s$ value; indicated in top-right are SMAF$_t$ and the average and standard deviation of SMAF$_s$. The average of SMAF$_s$ is greater than SMAF$_t$; this is a result of the lower limit of SMAF$_s$, which is by definition 1. Especially in low-melt regions, summers with high SMAF$_s$ have a larger effect on its average than on SMAF$_t$.

These locations were selected to illustrate the different SMAF regimes. On Larsen C ice shelf (Fig. 3f), SMAF leads to an increase in surface melt by a relatively constant factor every year, characterized by a low standard deviation of SMAF$_s$. This is different from e.g. Amery ice shelf (Fig. 3c), where SMAF$_s$ varies strongly from year to year (high standard deviation of SMAF$_s$). For the other locations, the standard deviation ranges between these extremes. Note that Larsen C and King Baudouin ice shelves have significant melt events outside of the summer months, because of regular Föhn events (Lenaerts et al., 2017; Wiesenekker et al., 2018). These are however not sensitive to SMAF, as they are not driven by short-wave radiation but rather by turbulent heat fluxes.

Figure 1b shows a decrease of SMAF$_s$ interannual variability with increasing melt. In low-melt regions ($<$ 100 mm w.e. yr^{-1}), melt is highly intermittent and the albedo remains generally high. If melt occurs, the albedo decreases significantly and surface melt increases relatively strongly, yielding large SMAF$_s$ values. In contrast, high-melt regions have a lower surface albedo to start with due to the higher prevailing temperatures; the albedo-lowering effect of melt is therefore less influential and melt is only slightly enhanced, leading to low SMAF$_s$ values and variability.

Figures 1 and 2 present the relationship between surface melt and SMAF. However, these figures also suggest there are more drivers determining SMAF. These are the subject of Sect. 4.1, where we identify climatic regions where SMAF is most active. Sec-

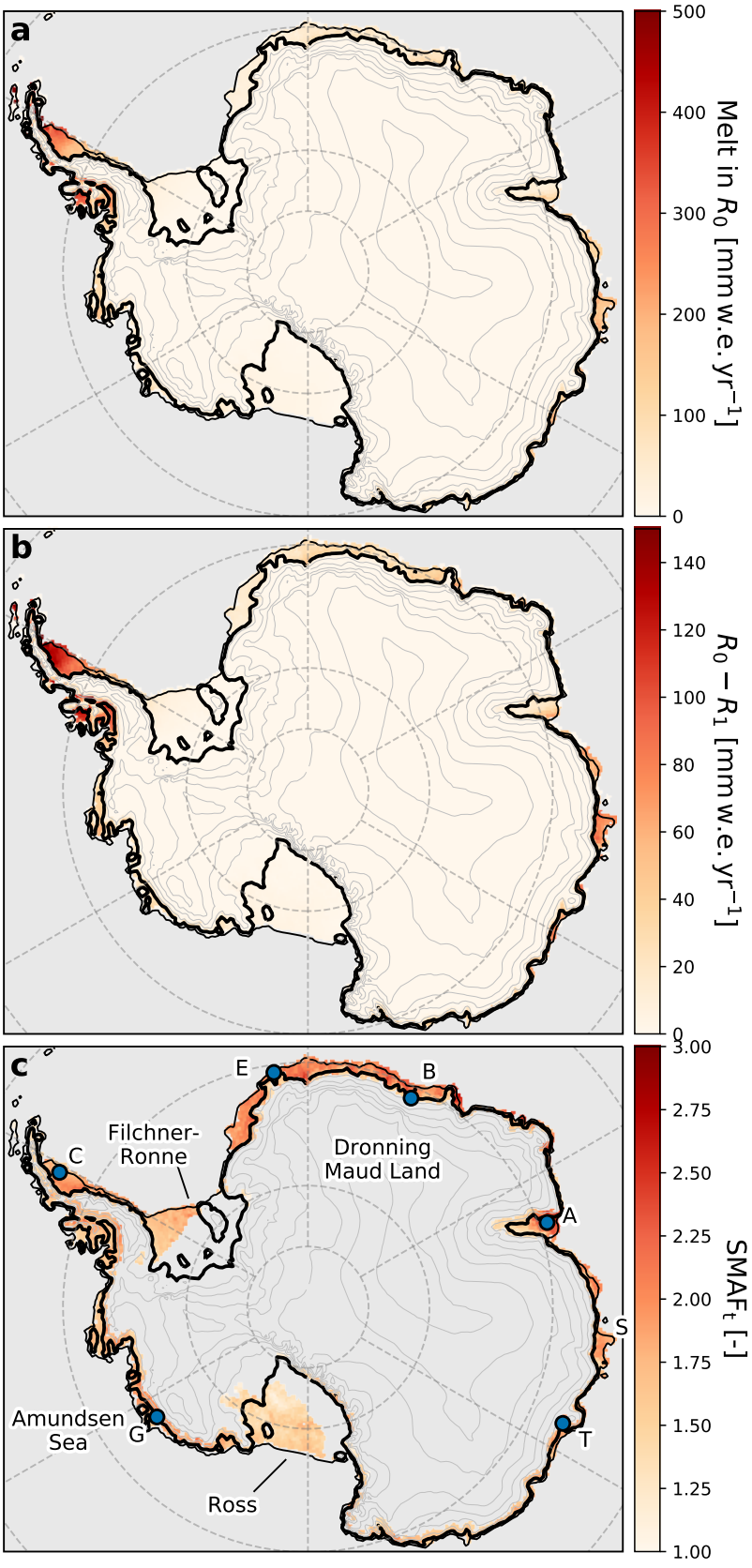

Figure 2. **(a)** Period-average seasonal surface melt rates modeled by RACMO2, with the full albedo parameterization (run R_0). **(b)** Difference in average seasonal surface melt rates between runs R_0 and R_1. **(c)** SMAF$_t$ for all grid points with period-average seasonal surface melt ≥ 5 mm w.e. Blue dots indicate sites for which Fig. 3 presents time series of surface melt: Ekström (E), King Baudouin (B), Amery (A), Totten (T), Getz (G) and Larsen C (C) ice shelves. Shackleton ice shelf is indicated with an S.

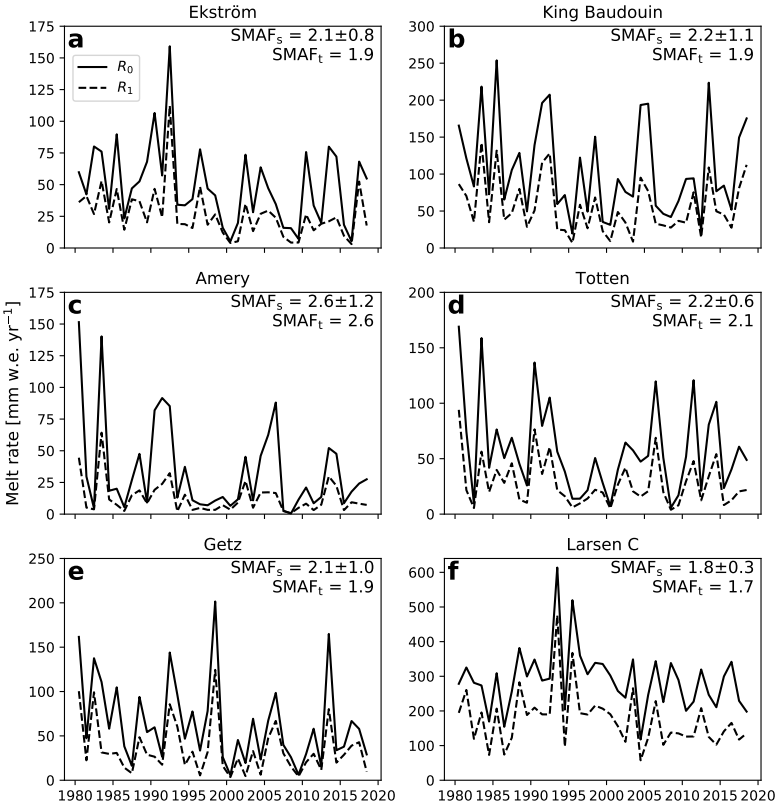

Figure 3. Time series of seasonal surface melt rates at various ice shelves around the Antarctic ice sheet (see Fig. 2c). Melt in R_0 is indicated with a solid line, in R_1 with a dashed line; the ratio between the two gives the seasonal $\mathrm{SMAF_s}$ value. Numbers in the top right corner are $\mathrm{SMAF_t}$, the average of $\mathrm{SMAF_s}$ and its standard deviation.

tion 4.2 focusses on how SMAF is related to the SEB on a daily timescale, for different regimes.

4 Discussion

4.1 Climatic drivers of SMAF

To understand the spatial patterns in Fig. 2c, we investigated the relationship between $\mathrm{SMAF_t}$ and several quantities: summer (Nov–Feb) air temperature, summer precipitation and seasonal surface melt rate. The most discernible pattern is observed in the correlation with temperature, which is therefore used below to describe large-scale climate drivers of $\mathrm{SMAF_t}$. Precipitation and surface melt are used to discuss SMAF on a sub-seasonal scale in Sect. 4.2.

Figure 4 presents the relation between $\mathrm{SMAF_t}$ and mean summer air temperature. It shows that the highest $\mathrm{SMAF_t}$ values are found in regions with an average summer air temperature of ∼265 K (defined as T_c), where $\mathrm{SMAF_t}$ reaches an average value of 1.9. This pattern is not very sensitive to the chosen period; it is similar if the time period is limited to an arbitrary 10-year or 20-year period throughout the total period (not shown). Its shape suggests a 'peak bandwidth' rather than a single peak value. Therefore, in the following we consider a 2 K bandwidth around T_c, i.e. $T_c = 265 \pm 2\,\mathrm{K}$.

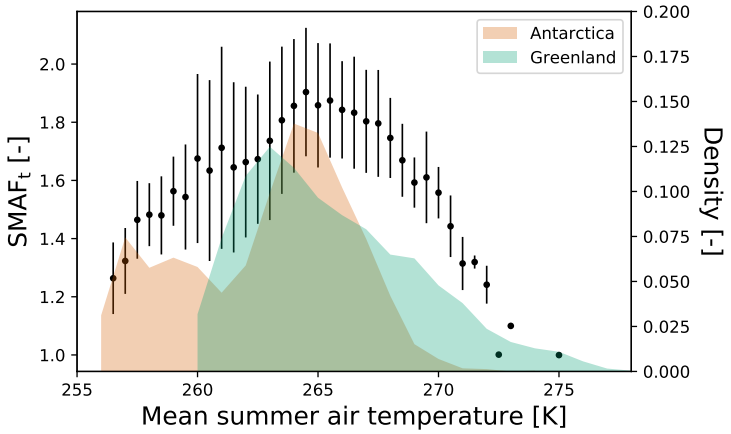

Figure 4. SMAF$_t$ as a function of binned (0.5 K) Nov–Feb average air temperature for all grid points with period-average seasonal surface melt of at least 5 mm w.e (black dots, lines indicate the standard deviation; the three rightmost dots have no lines because there is only 1 data point within the temperature bin). **Right axis** The shading indicates the normalized distribution of average summer air temperature for all grid points with period-average seasonal surface melt of at least 5 mm w.e. in Antarctica (orange, Nov–Feb) and in Greenland (green, accumulation zone only, May–Aug, Noël et al. (2018)).

In regions with temperatures above or below T_c, SMAF$_t$ gradually decreases to 1. In the colder regions ($T < 263$ K), surface melt rates are generally low (mostly < 30 mm w.e. yr^{-1}) and SMAF only moderately enhances surface melt (∼40–50%). In warmer regions ($T > 267$ K), such as the AP, SMAF is also less important for surface melt; due to the relatively mild conditions, the contribution of turbulent heat fluxes is more important to melt energy than absorption of short-wave radiation. This causes melt events that are less affected by the surface albedo, limiting the influence of SMAF. This is discussed in more detail in Sect. 4.2.

Figure 5 shows the spatial distribution of the deviation of average summer air temperature from T_c in Antarctica (Fig. 5a) and Greenland (Fig. 5b, Noël et al. (2018), discussed in Sect. 4.3). The Ross, Filchner-Ronne and Amery ice shelves extend far to the south and are the coldest areas which experience surface melt in Antarctica, with average summer air temperatures of 260 K and lower. These ice shelves represent the left tail of the temperature–SMAF$_t$ relation (Fig. 4), where SMAF has a limited effect on surface melt rates. The AP is the warmest region of Antarctica, with average summer air temperatures of 270 K and higher. It is located in the right tail of the temperature–SMAF$_t$ relation, where surface melt is semi-continuous, mainly driven by high air temperatures, and SMAF is also of limited importance for surface melt rates.

The remaining, smaller ice shelves in East and West Antarctica experience average summer air temperatures around T_c, displayed in white in Fig. 5a, with the 2 K bandwidth indicated with red contours. This indicates that SMAF is currently significantly (∼doubling) enhancing surface melt on ice shelves all around the AIS. In this high-SMAF regime, surface melt is an intermittent process; the meteorological circumstances that favor SMAF are identified in the next section.

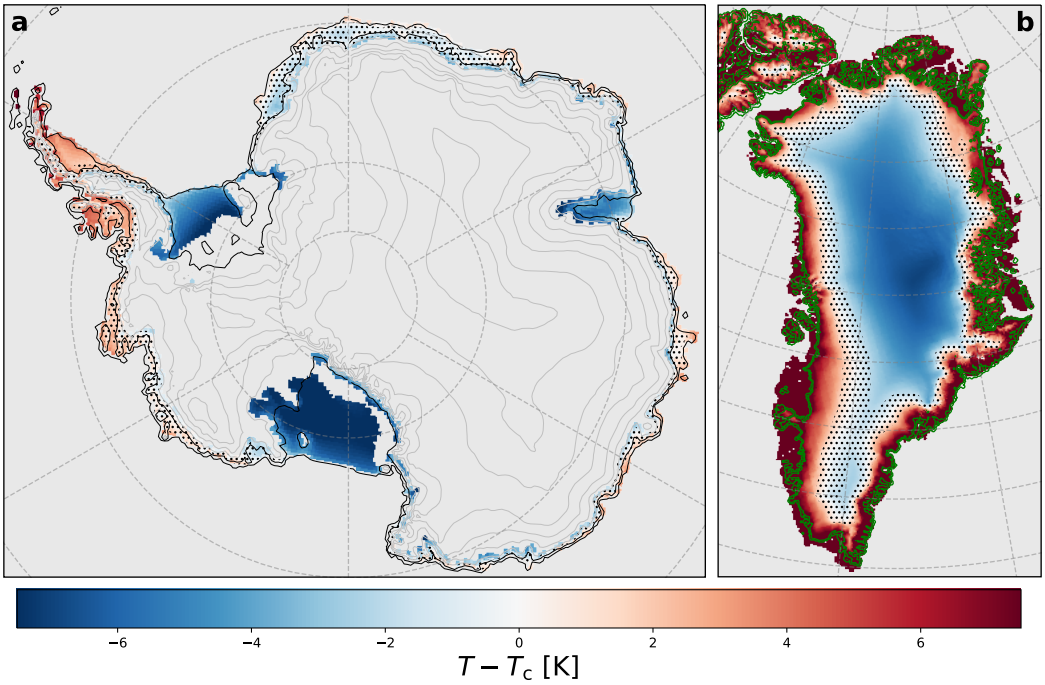

Figure 5. Temperature deviation from $T_c \equiv 265\,\mathrm{K}$, the temperature at which SMAF plateaus (see Fig. 4), for Antarctica (**a**) and Greenland (**b**). Blue areas indicate regions where SMAF will become increasingly important when air temperatures rise. White areas indicate regions where SMAF is now enhancing surface melt the most. Red areas indicate regions where air temperatures / melt are too high for an optimal SMAF. Black dots indicate the 2 K bandwidth around T_c, the green contour in (**b**) indicates the ice sheet margin (Noël et al., 2018).

4.2 SMAF and its connection to the SEB

To investigate SMAF and its drivers more closely, we compare summers with different SMAF values at four locations: King Baudouin ice shelf, Ross ice shelf, Larsen C ice shelf and Amery ice shelf (see Fig. 2c for locations). These locations were selected because they represent different SMAF regimes: moderate temperature, strong SMAF (King Baudouin, Fig. 6), high temperature, weak SMAF (Larsen C, Fig. 7), low temperature, weak SMAF (Ross, Fig. 8), and low temperature, strong SMAF (Amery, Fig. 9).

Figure 6 shows melt-season time series for a location on King Baudouin ice shelf, located in coastal Dronning Maud Land, (indicated by 'B' in Fig. 2c) in a moderate-temperature, strong-SMAF region (Fig. 5a). Figure 3b has shown that in this location, $\mathrm{SMAF_s}$ experiences a large interannual variability. Figure 6 shows daily cumulative surface melt (**a,e**), precipitation (**b,f**), the surface energy balance components (SEB, **c,g**) and temperature and albedo (**d,h**) for experiments R_0 and R_1 (see Sect. 2.2). In the melt season 2002–03, around 15 Dec, a melt episode occurs immediately after a strong precipitation event (Fig. 6a and b). Because of refreezing, the albedo drops from 0.9 to ∼0.75 (Fig. 6d). As no more significant snowfall events follow, the albedo remains low for the remainder of the season, resulting in significantly elevated $\mathrm{SW_{net}}$ values (Fig. 6c) and a prolonged period of surface melt in R_0. The surface albedo is not reset to that of new snow until the end of the melt season. As grain growth by refreezing is inactive in R_1, the decrease in albedo after the melt event is smaller; it stabilizes at ∼0.82. As the surface now reflects more solar radiation, $\mathrm{SW_{net}}$ is significantly lower and melt ceases af-

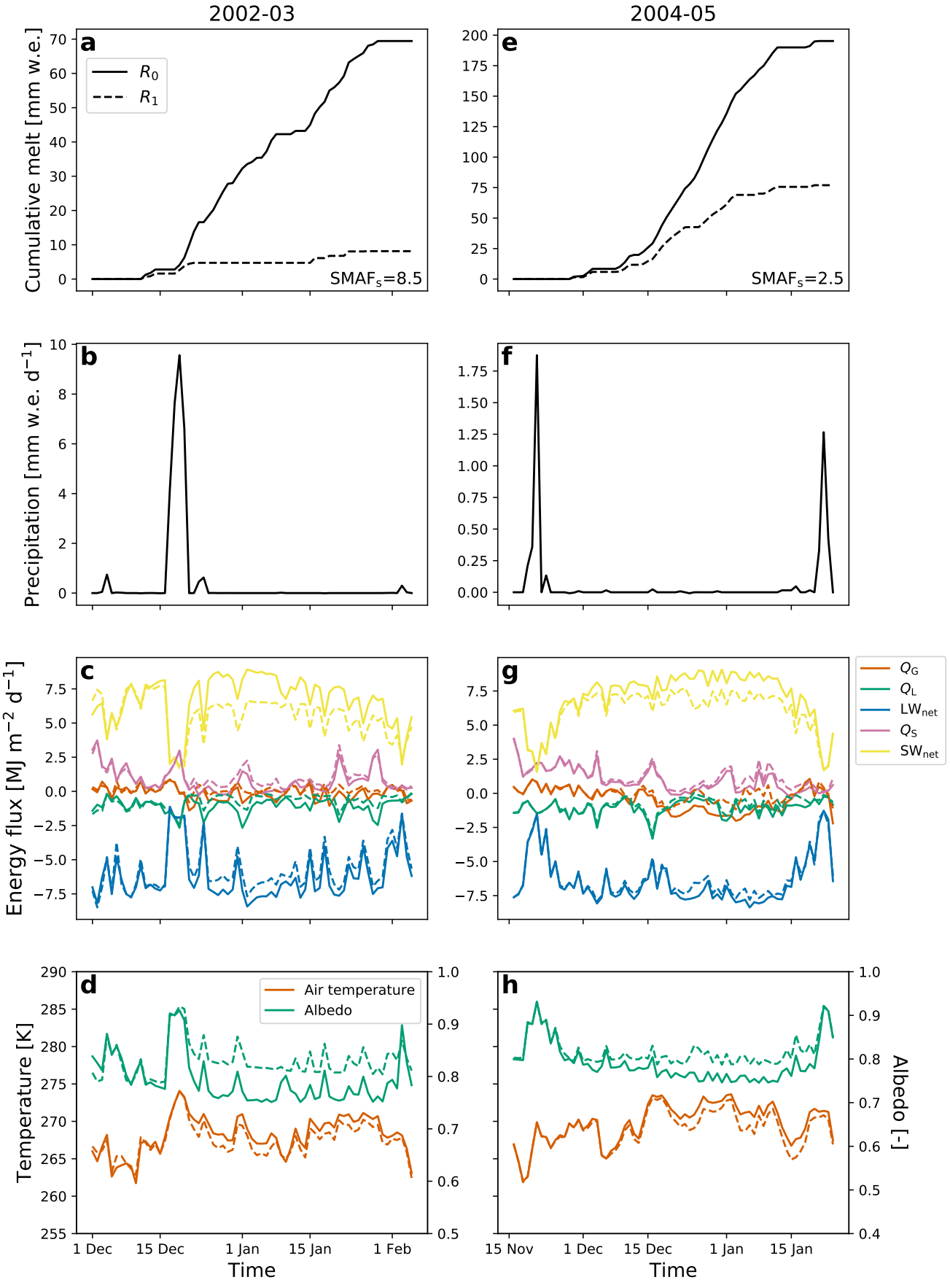

Figure 6. Time series of daily totals of **a,e** surface melt, **b,f** precipitation, **c,g** fluxes of surface energy balance components, and **d,h** average temperature and surface albedo, during the summer of 2002–03 (**a-d**) and 2004–05 (**e-h**) at King Baudouin ice shelf, Dronning Maud Land, East Antarctica (see Fig. 2c, indicated by B). In all panels solid lines indicate R_0 and dashed lines indicate R_1.

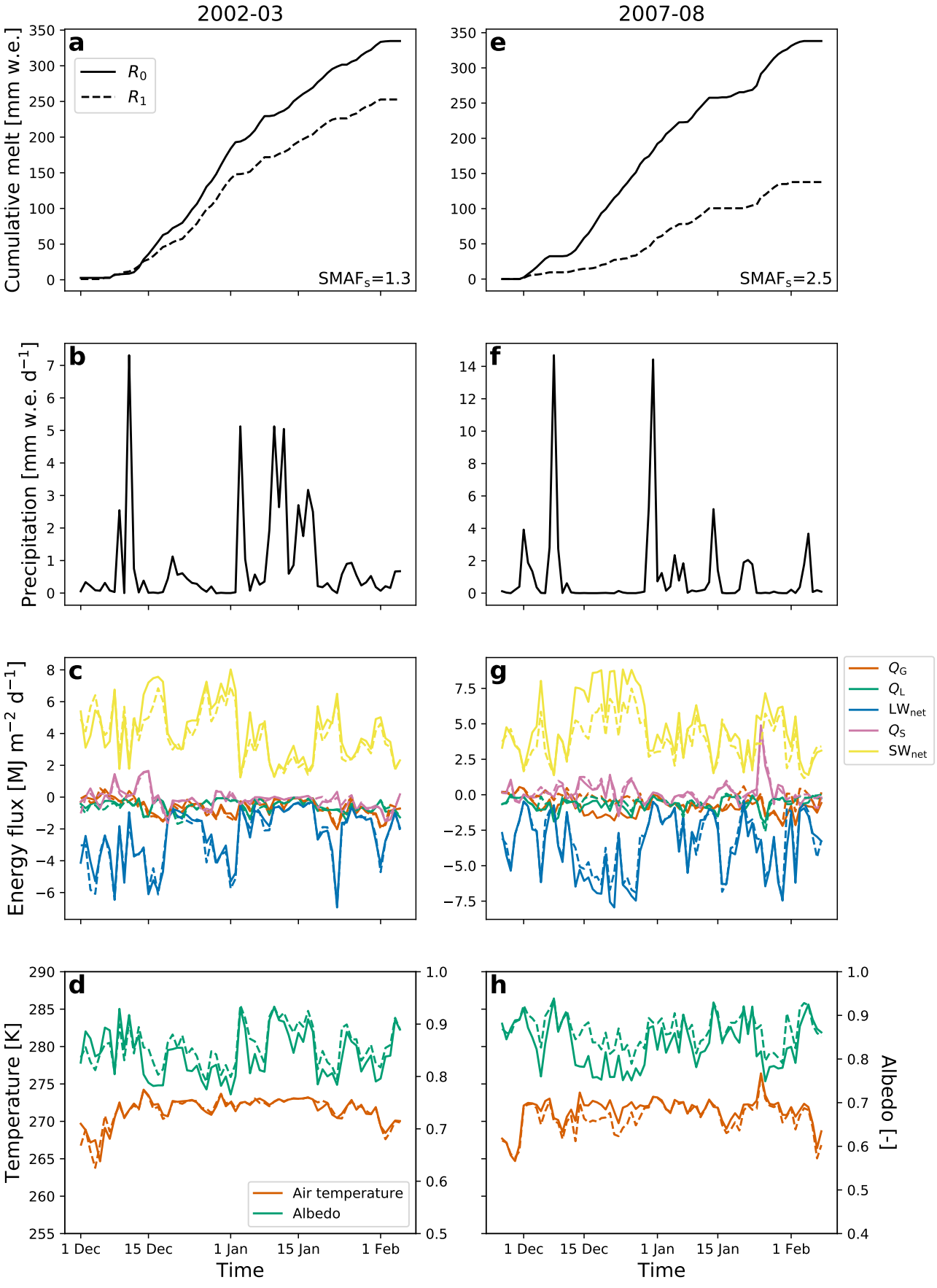

Figure 7. Same as Fig. 6 for Larsen C ice shelf, Antarctic Peninsula (see Fig. 2c, indicated by C).

ter the first melt event following the precipitation event. In R_0 melt totaled ∼70 mm w.e. during this season, while in R_1 it totaled only 8 mm w.e., yielding a high $\mathrm{SMAF_s}$ value of 8.5 (Fig. 6a).

At the same location but two seasons later (2004–05), a similar dry period occurred (Fig. 6e-h). Contrary to 2002–03, melt did not start immediately after the last significant snowfall event. Rather, the albedo decreases steadily because of dry snow metamorphism in both R_0 and R_1. Before the first melt of the season, the albedo had decreased to ∼0.82 in both runs. Similar to 2002–03, the albedo decreases more in R_0 than in R_1 during the melt event. However the effect of SMAF is now less pronounced than in 2002–03 because the albedo was already lowered, making the additional contribution of refrozen snow less important. The difference in $\mathrm{SW_{net}}$ is therefore also smaller, as well as the difference in surface melt rates throughout the season. The total 2004–05 surface melt amounts are ∼200 mm w.e. in R_0 and ∼80 mm w.e. in R_1, giving a $\mathrm{SMAF_s}$ of 2.5 (Fig. 6e).

Figure 7 shows results for a location on Larsen C ice shelf in the AP (indicated by 'C' in Fig. 2c), a region that experiences relatively high surface melt rates and higher temperatures than King Baudouin ice shelf, due to its more northerly location. Melt is enhanced by SMAF most efficiently between 15 Dec 2007 and 1 Jan 2008, during a prolonged dry period (Fig. 7e and f). The subsequent difference in albedo (Fig. 7h) resulted in significantly more absorption of solar radiation during this period (Fig. 7g) while temperatures were high enough to sustain surface melt. The absence of such a dry period in 2002–03 prevented SMAF from affecting surface melt as efficiently. Furthermore, the air temperature is close to the melting point throughout the season, which allowed sustained surface melt in both R_0 and R_1 runs. In the end, SMAF enhanced surface melt by only ∼30 % compared to ∼140 % in 2007–08, which again underlines the importance of dry periods for the effectiveness of SMAF. The effect is considerably smaller than on King Baudouin ice shelf (Fig. 6) because of the higher temperature on Larsen C, which allows for surface melt to proceed even in the absence of SMAF (R_1). This also explains the smaller interannual variability that is observed in Fig. 3f.

Figure 8 shows results for a location on Ross ice shelf, the largest ice shelf in Antarctica (see Fig. 2c). Due to its southerly location, temperatures are significantly lower than on King Baudouin ice shelf and, therefore, melt is more intermittent and less extensive. Although in 2007–08 (Fig. 8e-h) the air temperature occasionally reaches the melting point, sustained melt does not occur. Melt is limited to short melt events during which SMAF is unable to enhance surface melt over a longer period. However, because melt energies are so low, small absolute melt differences still induce a significant $\mathrm{SMAF_s}$ value for this season. In another year (2002–03), there was one significant melt event without any melt enhancement because of SMAF (Fig. 8a). Figure 8c shows that during the melt event, both $\mathrm{SW_{net}}$ and $\mathrm{LW_{net}}$ are approaching zero, indicating heavily overcast conditions. Melt energy is for an important part provided by Q_S, which is insensitive to surface albedo. As a result, SMAF did not enhance surface melt during this event.

Figure 9 shows daily melt, precipitation, SEB, temperature and albedo for a location on Amery ice shelf, East Antarctica (indicated by 'A' in Fig. 2c), which experiences relatively low average temperatures for its latitude. The first season (panels a–d) represents the high-SMAF summer 2004–05 without a prolonged dry period; even the precipitation event on 30 Dec was not able to sufficiently reset the surface albedo. During this event, melt continued because of the persistent high temperature and with it high Q_S. As a result the new snow was quickly removed from the surface. The difference in $\mathrm{SW_{net}}$ in the following days is sufficient to cause high $\mathrm{SMAF_s}$. In the summer of 2005–06 (panels e–h) an even higher $\mathrm{SMAF_s}$ occurs, resulting from a long dry episode. A remarkably large difference in air temperature is observed (Fig. 9h) during the persistent melt episode in R_0 which is absent in R_1. This is caused by persistently higher surface temperatures, following larger $\mathrm{SW_{net}}$ and refreezing.

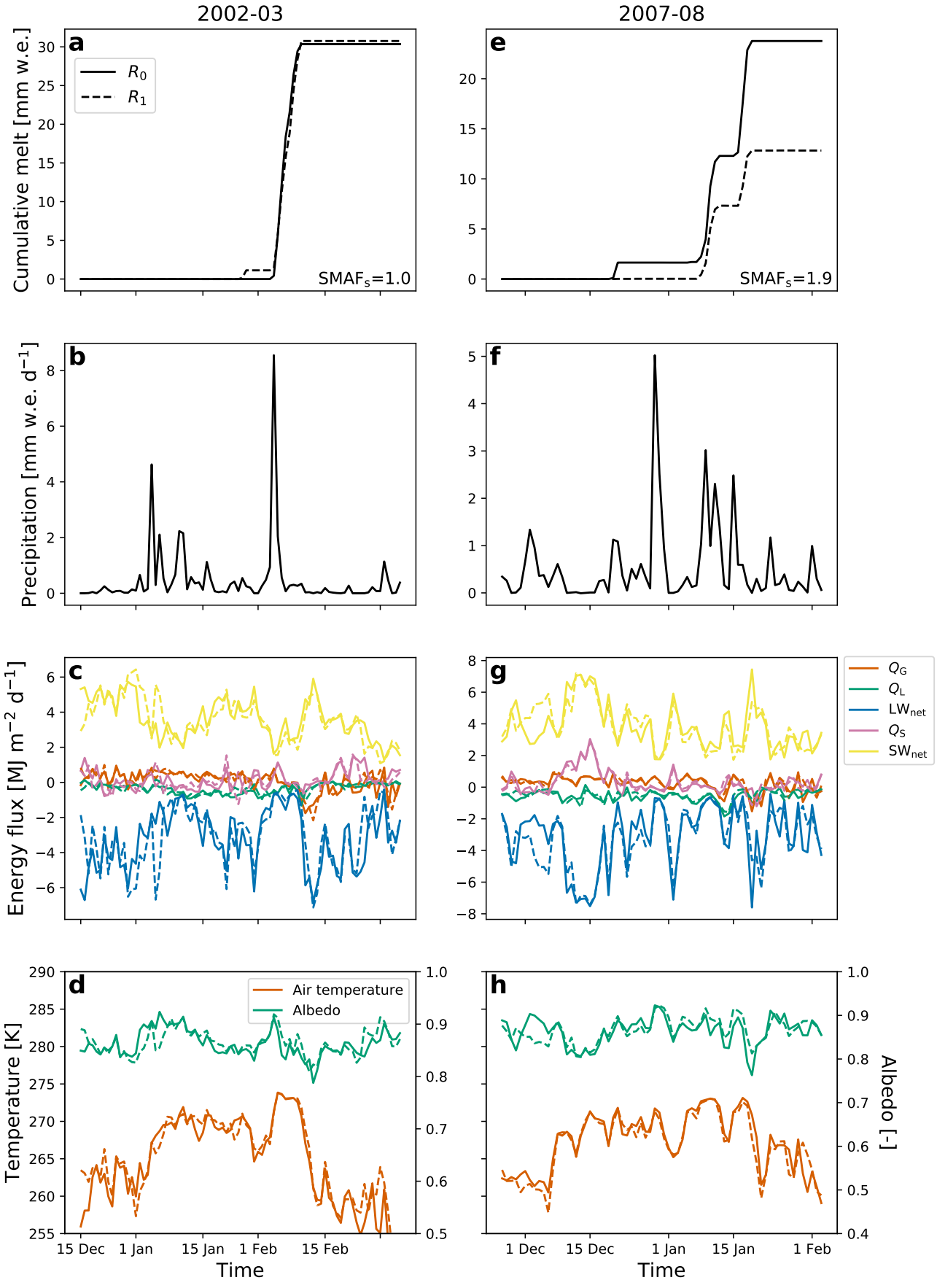

Figure 8. Same as Fig. 6 for Ross ice shelf (see Fig. 2c).

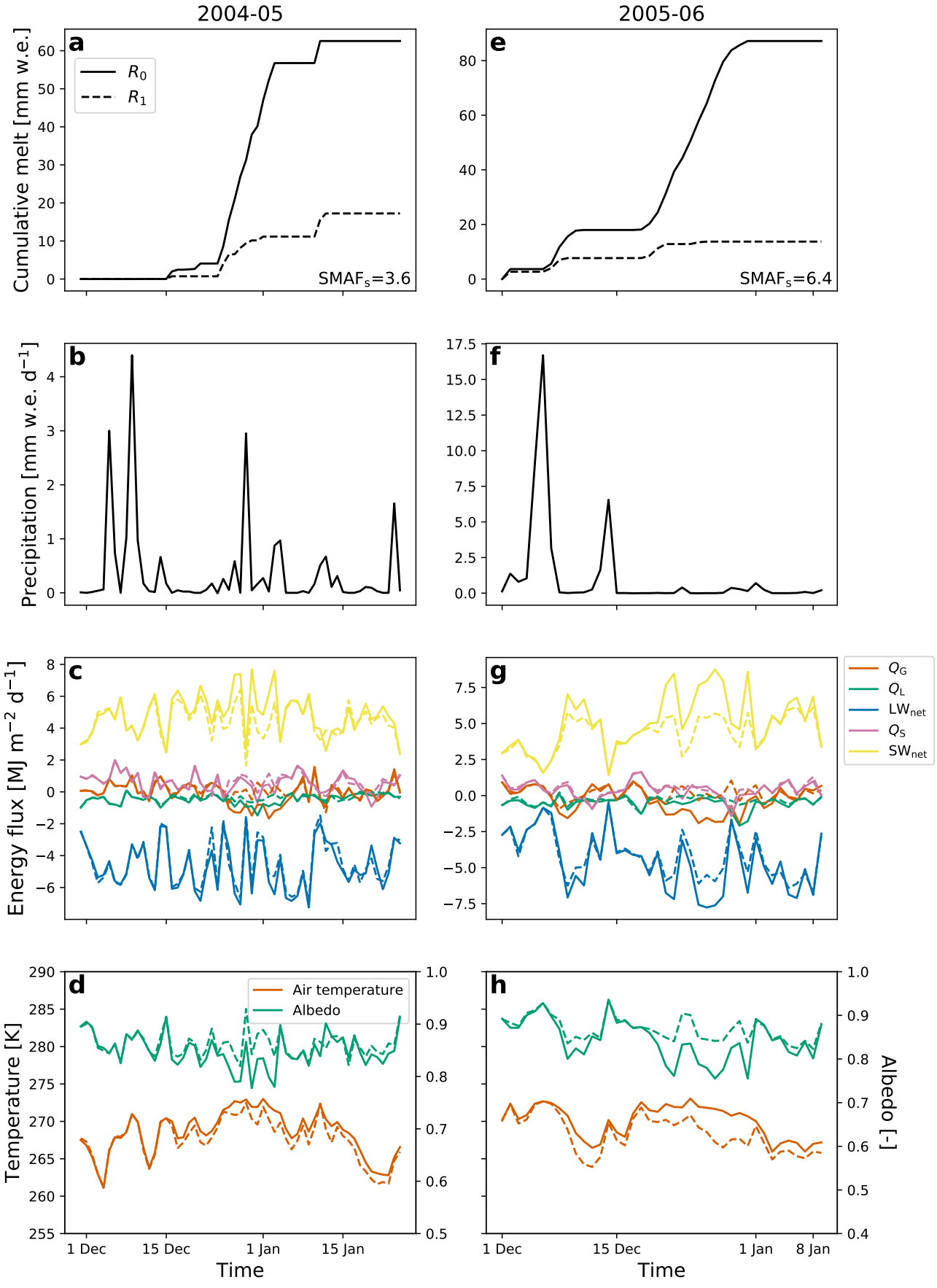

Figure 9. Same as Fig. 6 for Amery ice shelf, Dronning Maud Land (see Fig. 2c, indicated by A).

These examples show the different meteorological circumstances that can lead to different SMAF values. The moderate-temperature regions have the highest $\mathrm{SMAF_t}$ values, because SMAF causes the albedo to be lowered sufficiently such that enhanced absorption of solar radiation causes continuous melt, which is absent in R_1. In warm regions, even in cases when the albedo is higher, melt continues in R_1 (see Fig. 7d). Finally, in cold regions, sustained melt does not occur because of the low temperatures. Melt is limited to single-day melt events instead, rendering SMAF unable to enhance surface melt for a prolonged period, resulting in small $\mathrm{SMAF_s}$ and $\mathrm{SMAF_t}$ values.

These examples illustrate that especially prolonged dry periods in temperate summer climates enable SMAF to greatly enhance summer melt amounts, due to the lack of snowfall resetting the surface albedo. Quantifying the correlation between dry periods and $\mathrm{SMAF_s}$ remains difficult. The exact timing of precipitation and early melt events is equally important: when dry snow metamorphism has already lowered the surface albedo before surface melt starts, SMAF is strongly reduced.

We conclude that, in order to properly simulate the Antarctic melt climate, a climate model must accurately represent surface albedo, precipitation timing and intensity, and air and snow temperature.

4.3 Outlook: Greenland and the future

The shaded areas in Fig. 4 indicate the normalized distributions of temperature for all grid points with period-average seasonal surface melt of at least 1 mm w.e. in Antarctica (orange) and in Greenland (green, accumulation zone only, Noël et al. (2018)). The Ross, Filchner-Ronne and Amery ice shelves correspond to the left peak of this distribution, where the impact of SMAF on surface melt rates is limited (Sect. 4.1). The right peak of this temperature distribution represents the remaining ice shelves along East and West Antarctica. The higher temperatures are a result of their more northerly location than the Ross, Filchner-Ronne and Amery ice shelves. This shows that in the current climate, the majority of melt points fall in a regime with moderate SMAF, with only few locations significantly above T_c.

In a warmer climate, the distributions in Fig. 4 will shift towards the right. The East Antarctic ice shelves, located in the right peak of the orange distribution, will slowly become less affected by SMAF. On the other hand, the Ross, Filchner-Ronne and Amery ice shelves, which are in the left peak of this distribution, will gradually be exposed to higher SMAF values. As SMAF will become more important on these ice shelves, surface melt will increase relatively more strongly in these regions than for example on coastal Dronning Maud Land ice shelves. This might negatively affect the stability of the ice shelves through processes such as increased firn saturation, increased ice temperatures and hydrofracturing, and therewith affects the future of the AIS (Trusel et al., 2015).

The temperature distribution of melt points in Greenland is shown in green shading in Fig. 4 (accumulation zone only, Noël et al. (2018)). The absence of large, flat ice shelves results in large differences with the distribution of Antarctica. The bulk of the Greenland distribution is centered around 260 K, which represents the high and flat interior accumulation zone. Figure 10 shows the melt–temperature relation for Antarctica and Greenland (accumulation zone only), relating the period-average summer melt and summer temperature (Nov–Feb for Antarctica, May–Aug for Greenland). The Greenland curve seems to be an extension of the Antarctica curve, suggesting that when temperatures increase in the southern hemisphere, the Antarctic melt climate will increasingly resemble the contemporary Greenland melt climate. Note also that the temperature–SMAF relationship (Fig. 4) is not very sensitive to the time period for which it is calculated (not shown). This suggests that this relationship might also be applicable to Greenland. In order to assess how SMAF might affect surface melt in Greenland, we there-

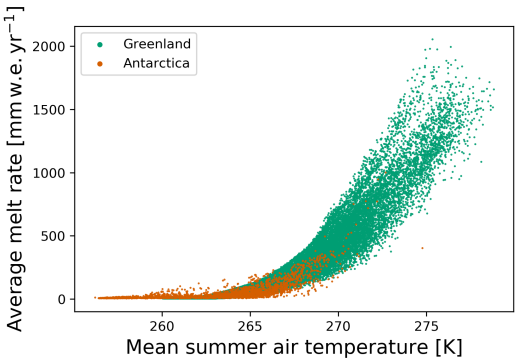

Figure 10. Period-average summer air temperature versus average seasonal surface melt for Greenland (green, accumulation zone only, Noël et al. (2018)) and Antarctica (orange) for all grid points with period-average seasonal surface melt of at least 5 mm w.e. Summer is defined as Nov–Feb in Antarctica and May–Aug in Greenland.

fore apply the temperature–SMAF relationship to the Greenland temperature distribution.

Figure 5b shows the temperature deviation from T_c for Greenland. Similar to Fig. 5a, white areas indicate the regions where SMAF is currently most optimal for enhancing surface melt, red areas are too warm for a strong SMAF, and blue areas are currently too cold. In the current climate and based on our results from the AIS, it shows that SMAF is active in a large part of the interior ice sheet in southern Greenland, and a narrow band in the middle-elevated accumulation zone around the rest of the ice sheet. In a warming climate, the SMAF region will migrate inland, corresponding to a right-ward shift of the green temperature distribution in Fig. 4. This leads to a rapid increase of the area being affected by SMAF when air temperatures over Greenland continue to rise.

5 Conclusions

In this study we investigate the spatial and temporal variability of the snowmelt–albedo feedback (SMAF) on the Antarctic ice sheet (AIS). This is done by performing two simulations with the regional atmospheric climate model RACMO2, covering the period 1979–2018. This model uses a parameterization that relates the surface albedo to the grain size of snow; by disabling the contribution of refrozen snow to albedo lowering, this allows us to explicitly model the effect of SMAF on surface melt. One simulation is performed with the full albedo parameterization (R_0), in the other simulation this refrozen-snow contribution is disabled (R_1). Following Jakobs et al. (2019), we define SMAF as the ratio of cumulative surface melt between these two simulations, a value of 1 indicating no effect, a value of X indicating that melt is enhanced X-fold because of SMAF.

We find that SMAF is spatially highly variable on the AIS, ranging from values close to 1 in cold, low-melt regions such as the Ross and Filchner-Ronne ice shelves, to values up to 3 in coastal Dronning Maud Land (Fig. 2). Relating $\mathrm{SMAF_t}$ to average summer (Nov–Feb) air temperature reveals a maximum around 265 K (T_c, Fig. 4). Many Antarctic ice shelves are located in the temperature regime where SMAF is currently optimal, except for the three largest ice shelves (Ross, Filchner-Ronne and Amery), which are too cold, and the entire Antarctic Peninsula (Fig. 5a), which is too warm.

Investigating the link between SMAF and the surface energy balance reveals that the timing of significant snowfall events with respect to surface melt is important. Seasonal SMAF is highest when melt occurs immediately after the last snowfall event at the onset of the melt season and in the absence of significant precipitation throughout the remainder of the season. The reason is that in this case the surface albedo is not reset to the new-snow value and enhanced melt occurs continuously. When snowfall is not immediately followed by surface melt, the surface albedo is lowered by dry snow metamorphism. The effect of refrozen snow on seasonal albedo is subsequently much smaller than in the previous example, and therefore SMAF is less important. In cold regions such as the Ross ice shelf, the air temperature is generally too low to accommodate continuous surface melt. When surface melt occurs, it is mostly constrained to a single melt day; as a result, SMAF is not able to significantly enhance surface melt. On Larsen C ice shelf, located in the mild AP, the air temperature is normally high enough to facilitate near-continuous surface melt; SMAF does enhance surface melt but it does not determine whether surface melt continues or ceases. This is contrary to moderate-temperature locations, where SMAF can be the determining factor for the start and continuation of surface melt.

Although a large part of Antarctica is currently too cold for an optimal SMAF, which occurs at $\sim 265\,\mathrm{K}$, rising temperatures in the future could expose even the largest ice shelves to a strong increase in surface melt because of SMAF. Applying the same threshold to the Greenland ice sheet shows that a large part of southern Greenland is in the SMAF-sensitive temperature regime (Fig. 5b), indicating that SMAF is an important driver for surface melt in that area.

Acknowledgments

This research has been supported by the Nederlandse Organisatie voor Wetenschappelijk Onderzoek (grant no. 866.15.204). Michiel van den Broeke acknowledges support from the Netherlands Earth System Science Centre (NESSC). We thank Brice Noël for carrying out the RACMO2.3p2 Greenland simulation. The data are available on `https://doi.org/10.5281/zenodo.3836044`. The authors declare no conflicts of interest.

References

Agosta, C., Amory, C., Kittel, C., Orsi, A., Favier, V., Gallée, H., ... Fettweis, X. (2019). Estimation of the antarctic surface mass balance using the regional climate model mar (1979-2015) and identification of dominant processes. *The Cryosphere*, *13*, 281-296. doi: 10.5194/tc-13-281-2012

Alexander, P. M., LeGrande, A. N., Fischer, E., Tedesco, M., Fettweis, X., Kelley, M., ... Schmidt, G. A. (2019). Simulated greenland surface mass balance in the giss modele2 gcm: Role of the ice sheet surface. *Journal of Geophysical Research: Earth Surface*, *124*, 750-765. doi: 10.1029/2018JF004772

Bindschadler, R., Choi, H., Wichlacz, A., Bingham, R., Bohlander, J., Brunt, K., ... Young, N. (2011). Getting around antarctica: new high-resolution mappings of the grounded and freely-floating boundaries of the antarctic ice sheet created for the international polar year. *The Cryosphere*, *5*, 569-588. doi: 10.5194/tc-5-569-2011

Bisiaux, M. M., Edwards, R., McConnell, J. R., Curran, M. A. J., Van Ommen, T. D., Smith, A. M., ... Taylor, K. (2012). Changes in black carbon deposition to antarctica from two high-resolution ice core records, 1850-2000 ad. *Atmospheric Chemistry and Physics*, *12*, 4107-4115. doi: 10.5194/acp-12-4107-2012

Braun, M., Humbert, A., & Moll, A. (2009). Changes of wilkins ice shelf over the past 15 years and inferences on its stability. *The Cryosphere*, *3*, 41-56. doi: 10.5194/tc-3-41-2009

Bromwich, D. H., Otieno, F. O., Hines, K. M., Manning, K. W., & Shilo, E. (2013).

Comprehensive evaluation of polar weather research and forecasting model performance in the antarctic. *Journal of Geophysical Research: Atmospheres*, *118*, 274-292. doi: 10.1029/2012JD018139

Cullather, R. I., Nowicki, S. M. J., Zhao, B., & Suarez, M. J. (2014). Evaluation of the surface representation of the greenland ice sheet in a general circulation model. *Journal of Climate*, *27*, 4835-4856. doi: 10.1175/JCLI-D-13-00635.1

ECMWF. (2008). IFS DOCUMENTATION - Cy33r1 - PART IV: PHYSICAL PROCESSES [Computer software manual]. Retrieved from `https://www.ecmwf.int/en/elibrary/9227-part-iv-physical-processes` ([Online; accessed 6 June 2019])

Ettema, J., Van den Broeke, M. R., Van Meijgaard, E., Van de Berg, W. J., Box, J. E., & Steffen, K. (2010). Climate of the greenland ice sheet using a high-resolution climate model - part 1: Evaluation. *The Cryosphere*, *4*, 511-527. doi: 10.5194/tc-4-511-2010

Gardner, A. S., & Sharp, M. J. (2010). A review of snow and ice albedo and the development of a new physically based broadband albedo parameterization. *Journal of Geophysical Research: Earth Surface*, *115*(F01009). doi: 10.1029/2009JF001444

Glasser, N. F., & Scambos, T. A. (2008). A structural glaciological analysis of the 2002 larsen b ice-shelf collapse. *Journal of Glaciology*, *54*(184), 3-16. doi: 10.3189/002214308784409017

Grenfell, T. C., Warren, S. G., & Mullen, P. C. (1994). Reflection of solar radiation by the antarctic snow surface at ultraviolet, visible, and near-infrared wavelengths. *Journal of Geophysical Research*, *99*(D9), 18669-18684. doi: 10.1029/94JD01484

Jakobs, C. L., Reijmer, C. H., Kuipers Munneke, P., König-Langlo, G., & Van den Broeke, M. R. (2019). Quantifying the snowmelt-albedo feedback at neumayer station, east antarctica. *The Cryosphere*, *13*, 1473-1485. doi: 10.5194/tc-13-1473-2019

Jakobs, C. L., Reijmer, C. H., Smeets, C. J. P. P., Trusel, L. D., Van de Berg, W. J., Van den Broeke, M. R., & Van Wessem, J. M. (2020). A benchmark dataset of in situ antarctic surface melt rates and energy balance. *Journal of Glaciology*, *66*(256), 291-302. doi: 10.1017/jog.2020.6

Jonsell, U. Y., Navarro, F. J., Bañón, M., Lapazaran, J. J., & Otero, J. (2012). Sensitivity of a distributed temperature-radiation index melt model based on aws observations and surface energy balance fluxes, hurd peninsula glaciers, livingston island, antarctica. *The Cryosphere*, *6*, 539-552. doi: 10.5194/tc-6-539-2012

King, J. C., Gadian, A., Kirchgaessner, A., Kuipers Munneke, P., Lachlan-Cope, T. A., Orr, A., ... Weeks, M. (2015). Validation of the summertime surface energy budget of larsen c ice shelf (antarctica) as represented in three high-resolution atmospheric models. *Journal of Geophysical Research: Atmospheres*, *120*, 1335-1347. doi: 10.1002/2014JD022604

Kingslake, J., Ely, J. C., Das, I., & Bell, R. E. (2017). Widespread movement of meltwater onto and across antarctic ice shelves. *Nature*, *544*, 349-352. doi: 10.1038/nature22049

Kuipers Munneke, P., Van den Broeke, M. R., Lenaerts, J. T. M., Flanner, M. G., Gardner, A. S., & Van de Berg, W. J. (2011). A new albedo parameterization for use in climate models over the antarctic ice sheet. *Journal of Geophysical Research: Atmospheres*, *116*(D05114). doi: 10.1029/2010JD015113

Lenaerts, J. T. M., Lhermitte, S., Drews, R., Ligtenberg, S. R. M., Berger, S., Helm, V., ... Pattyn, F. (2017). Meltwater produced by wind-albedo interaction stored in an east antarctic ice shelf. *Nature Climate Change*, *7*, 58-62. doi: 10.1038/nclimate3180

Lenaerts, J. T. M., Van den Broeke, M. R., Déry, S. J., Van Meijgaard, E., Van de

Berg, W. J., Palm, S. P., & Sanz Rodrigo, J. (2012). Modeling drifting snow in antarctica with a regional climate model: 1. methods and model evaluation. *Journal of Geophysical Research: Atmospheres*, *117*(D05108). doi: 10.1029/2011JD016145

Marquetto, L., Kaspari, S., & Simões, J. C. (2020). Refractory black carbon (rbc) variability in a 47-year west antarctic snow and firn core. *The Cryosphere*, *14*, 1537-1554. doi: tc-14-1537-2020

Massom, R. A., Scambos, T. A., Bennetts, L. G., Reid, P. A., Squire, V. A., & Stammerjohn, S. E. (2018). Antarctic ice shelf disintegration triggered by sea ice loss and ocean swell. *Nature*, *558*, 383-389. doi: 10.1038/s41586-018-0212-1

Morlighem, M., Rignot, E., Binder, T., Blankenship, D. D., Drews, R., Eagles, G., ... Young, D. A. (2020). Deep glacial troughs and stabilizing ridges unveiled beneath the margins of the antarctic ice sheet. *Nature Geoscience*, *13*, 132-137. doi: 10.1038/s41561-019-0510-8

Noël, B. P. Y., Van de Berg, W. J., Van Wessem, J. M., Van Meijgaard, E., Van As, D., Lenaerts, J. T. M., ... Van den Broeke, M. R. (2018). Modelling the climate and surface mass balance of polar ice sheets using racmo2, part 1: Greenland (1958-2016). *The Cryosphere*, *12*, 811-831. doi: 10.5194/tc-12-811-2018

Padman, L., Costa, D. P., Dinniman, M. S., Fricker, H. A., Goebel, M. E., Huckstadt, L. A., ... Van den Broeke, M. R. (2012). Oceanic controls on the mass balance of wilkins ice shelf, antarctica. *Journal of Geophysical Research*, *117*(C01010). doi: 10.1029/2011JC007301

Pritchard, H. D., Ligtenberg, S. R. M., Fricker, H. A., Vaughan, D. G., Van den Broeke, M. R., & Padman, L. (2012). Antarctic ice-sheet loss driven by basal melting of ice shelves. *Nature*, *484*, 502-505. doi: 10.1038/nature10968

Reijmer, C. H., Van Meijgaard, E., & Van den Broeke, M. R. (2005). Evaluation of temperature and wind over antarctica in a regional atmospheric climate model using 1 year of automatic weather station data and upper air observations. *Journal of Geophysical Research*, *110*(D04103). doi: 10.1029/2004JD005234

Rott, H., Müller, F., Nagler, T., & Floricioiu, D. (2011). The imbalance of glaciers after disintegration of larsen-b ice shelf, antarctic peninsula. *The Cryosphere*, *5*, 125-134. doi: 10.5194/tc-5-125-2011

Scambos, T. A., Bohlander, J. A., Shuman, C. A., & Skvarca, P. (2004). Glacier acceleration and thinning after ice shelf collapse in the larsen b embayment, antarctica. *Geophysical Research Letters*, *31*(L18402). doi: 10.1029/2004GL020670

Shepherd, A., Ivins, E. R., Rignot, E., Smith, B., Van den Broeke, M. R., Velicogna, I., ... Wouters, B. (2018). Mass balance of the antarctic ice sheet from 1992 to 2017. *Nature*, *558*, 219-222. doi: 10.1038/s41586-018-0179-y

Souverijns, N., Gossart, A., Demuzere, M., Lenaerts, J. T. M., Medley, B., Gorodetskaya, I. V., ... Van Lipzig, N. P. M. (2019). A new regional climate model for polar-cordex: Evaluation of a 30-year hindcast with cosmo-clm^2 over antarctica. *Journal of Geophysical Research: Atmospheres*, *124*, 1405-1427. doi: 10.1029/2018JD028862

Trusel, L. D., Frey, K. E., Das, S. B., Karnauskas, K. B., Kuipers Munneke, P., Van Meijgaard, E., & Van den Broeke, M. R. (2015). Divergent trajectories of antarctic surface melt under two twenty-first-century climate scenarios. *Nature Geoscience*, *8*, 927-934. doi: 10.1038/NGEO2563

Turner, J., Orr, A., Gudmundsson, G. H., Jenkins, A., Bingham, R. G., Hillenbrand, C.-D., & Bracegirdle, T. J. (2017). Atmosphere-ocean-ice interactions in the amundsen sea embayment, west antarctica. *Reviews of Geophysics*, *55*, 235-276. doi: 10.1002/2016RG000532

Undén, P., Rontu, L., Järvinen, H., Lynch, P., Calvo, J., Cats, G., ... Tijm, A. (2002). Hirlam-5 scientific documentation [Computer software manual].

Retrieved from `http://hirlam.org/index.php/hirlam-documentation/doc\_download/308-unden-et-al-2002` ([Online; accessed 25 January 2017])

Van Dalum, C. T., Van de Berg, W. J., Libois, Q., Picard, G., & Van den Broeke, M. R. (2019). A module to convert spectral to narrowband snow albedo for use in climate models: Snowbal v1.2. *Geoscientific Model Development*, *12*, 5157-5175. doi: 10.5194/gmd-12-5157-2019

Van de Berg, W. J., & Medley, B. (2016). Brief communication: Upper-air relaxation in racmo2 significantly improved modelled interannual surface mass balance variability in antarctica. *The Cryosphere*, *10*, 459-463. doi: 10.5194/tc-10-459-2016

Van den Broeke, M. R. (2005). Strong surface melting preceded collapse of antarctic peninsula ice shelf. *Geophysical Research Letters*, *32*(L12815). doi: 10.1029/2005GL023247

Van den Broeke, M. R., Reijmer, C. H., Van As, D., Van de Wal, R. S. W., & Oerlemans, J. (2005). Seasonal cycles of antarctic surface energy balance from automatic weather stations. *Annals of Glaciology*, *41*, 131-139. doi: 10.3189/172756405781813168

Van den Broeke, M. R., Van As, D., Reijmer, C. H., & Van de Wal, R. S. W. (2005). Sensible heat exchange at the antarctic snow surface: a study with automatic weather stations. *International Journal of Climatology*, *25*, 1081-1101. doi: 10.1002/joc.1152

Van Kampenhout, L., Lenaerts, J. T. M., Lipscomb, W. H., Sacks, W. J., Lawrence, D. M., Slater, A. G., & Van den Broeke, M. R. (2017). Improving the representation of polar snow and firn in the community earth system model. *Journal of Advances in Modeling Earth Systems*, *9*, 2583-2600. doi: 10.1002/2017MS000988

Van Wessem, J. M., Van de Berg, W. J., Noël, B. P. Y., Van Meijgaard, E., Birnbaum, G., Jakobs, C. L., ... Van den Broeke, M. R. (2018). Modelling the climate and surface mass balance of polar ice sheets using RACMO2, part 2: Antarctica (1979-2016). *The Cryosphere*, *12*, 1479-1498. doi: 10.5194/tc-2017-202

Warren, S. G., & Clarke, A. D. (1990). Soot in the atmosphere and snow surface of antarctica. *Journal of Geophysical Research*, *95*(D2), 1811-1816. doi: 10.1029/JD095iD02p01811

Wiesenekker, J. M., Kuipers Munneke, P., Van den Broeke, M. R., & Smeets, C. J. P. P. (2018). A multidecadal analysis of föhn winds over larsen c ice shelf from a combination of observations and modeling. *Atmosphere*, *9*, 172. doi: 10.3390/atmos9050172

Wiscombe, W. J., & Warren, S. G. (1980). A model for the spectral albedo of snow. i: Pure snow. *Journal of the Atmospheric Sciences*, *37*, 2712-2733. doi: 10.1175/1520-0469(1980)037⟨2712:AMFTSA⟩2.0.CO;2

Wouters, B., Martin-Español, A., Helm, V., Flament, T., Van Wessem, J. M., Ligtenberg, S. R. M., ... Bamber, J. L. (2015). Dynamic thinning of glaciers on the southern antarctic peninsula. *Science*, *348*(6237), 899-903. doi: 10.1126/science.aaa5727